Class. Quantum Grav. **24** (2007) 5767–5775 doi:10.1088/0264-9381/24/23/003

Status of coalescing binaries search activities in Virgo

F Acernese[1], P Amico[2], M Alshourbagy[3], F Antonucci[4], S Aoudia[5], P Astone[4], S Avino[1], D Babusci[6], G Ballardin[7], F Barone[1], L Barsotti[3], M Barsuglia[8], Th S Bauer[9], F Beauville[10], S Bigotta[3], S Birindelli[3], M A Bizouard[8], C Boccara[11], F Bondu[5], L Bosi[2], C Bradaschia[3], S Braccini[3], J F J van den Brand[9], A Brillet[5], V Brisson[8], D Buskulic[10], E Calloni[1], E Campagna[12], F Carbognani[7], F Cavalier[8], R Cavalieri[7], G Cella[3], E Cesarini[12], E Chassande-Mottin[5], N Christensen[7], C Corda[3], A Corsi[4], F Cottone[2], A-C Clapson[8], F Cleva[5], J-P Coulon[5], E Cuoco[7], A Dari[2], V Dattilo[7], M Davier[8], M del Prete[3], R De Rosa[1], L Di Fiore[1], A Di Virgilio[3], B Dujardin[5], A Eleuteri[1], M Evans[7], I Ferrante[3], F Fidecaro[3], I Fiori[7], R Flaminio[7,10], J-D Fournier[5], S Frasca[4], F Frasconi[3], L Gammaitoni[2], F Garufi[1], E Genin[7], A Gennai[3], A Giazotto[3], G Giordano[6], L Giordano[1], R Gouaty[10], D Grosjean[10], G Guidi[12], S Hamdani[7], S Hebri[7], H Heitmann[5], P Hello[8], D Huet[7], S Karkar[10], S Kreckelbergh[8], P La Penna[7], M Laval[5], N Leroy[8], N Letendre[10], B Lopez[7], Lorenzini[12], V Loriette[11], G Losurdo[12], J-M Mackowski[13], E Majorana[2], C N Man[5], M Mantovani[3], F Marchesoni[2], F Marion[10], J Marque[7], F Martelli[12], A Masserot[10], M Mazzoni[12], L Milano[1], F Menzinger[7], C Moins[7], J Moreau[11], N Morgado[13], B Mours[10], F Nocera[7], C Palomba[2], F Paoletti[3,7], S Pardi[1], A Pasqualetti[7], R Passaquieti[3], D Passuello[3], F Piergiovanni[12], L Pinard[13], R Poggiani[3], M Punturo[2], P Puppo[4], S van der Putten[9], K Qipiani[1], P Rapagnani[4], V Reita[11], A Remillieux[13], F Ricci[4], I Ricciardi[1], P Ruggi[7], G Russo[1], S Solimeno[1], A Spallicci[5], M Tarallo[3], M Tonelli[3], A Toncelli[3], E Tournefier[10], F Travasso[2], C Tremola[3], G Vajente[3], D Verkindt[12], F Vetrano[12], A Viceré[12], J-Y Vinet[5], H Vocca[2] and M Yvert[10]

[1] INFN, Sezione di Napoli and/or Università di Napoli 'Federico II' Complesso Universitario di Monte S Angelo Via Cintia, I-80126 Napoli, Italia and/or Università di Salerno Via Ponte Don Melillo, I-84084 Fisciano (Salerno), Italy
[2] INFN Sezione di Perugia and/or Università di Perugia, Via A Pascoli, I-06123 Perugia, Italy
[3] INFN, Sezione di Pisa and/or Università di Pisa, Via Filippo Buonarroti, 2 I-56127 PISA, Italy
[4] INFN, Sezione di Roma and/or Università 'La Sapienza', P le A Moro 2, I-00185, Roma
[5] Department Artemis—Observatoire de la Côte d'Azur, BP 42209, 06304 Nice Cedex 4, France
[6] INFN, Laboratori Nazionali di Frascati Via E Fermi, 40, I-00044 Frascati (Rome), Italy
[7] European Gravitational Observatory (EGO), Via E Amaldi, I-56021 Cascina (PI), Italy
[8] Laboratoire de l'Accélérateur Linéaire, LAL, Univ Paris-Sud, IN2P3/CNRS, Orsay, France
[9] National Institute for Nuclear Physics and High Energy Physics, NL-1009 DB Amsterdam and/or Vrije Universiteit, NL-1081 HV Amsterdam, The Netherlands
[10] Laboratoire d'Annecy-le-Vieux de physique des particules (LAPP), IN2P3/CNRS, Université de Savoie, BP 110, F-74941, Annecy-le-Vieux, CEDEX, France
[11] ESPCI 10, rue Vauquelin, 75005 Paris, France
[12] INFN, Sezione Firenze/Urbino Via G Sansone 1, I-50019 Sesto Fiorentino and/or Università di Firenze, Largo E Fermi 2, I-50125 Firenze and/or Università di Urbino, Via S Chiara, 27 I-61029 Urbino, Italy
[13] LMA 22, Boulevard Niels Bohr 69622, Villeurbanne, Lyon Cedex, France

0264-9381/07/235767+09$30.00

Received 21 May 2007, in final form 17 October 2007
Published 21 November 2007
Online at stacks.iop.org/CQG/24/5767

Abstract
The interferometric gravitational wave detector Virgo is undergoing an advanced phase of its commissioning, during which short runs are routinely performed, in which data are analyzed online and offline, searching for signals from coalescing binary systems. In this report we present the progress of the coalescing binaries search activities in Virgo, and we describe details of the detection pipeline including hardware injections, vetoes, and parameter estimation, using recent data taking.

PACS numbers: 04.80.Nn, 95.55.Ym

(Some figures in this article are in colour only in the electronic version)

1. Introduction

The interferometric gravitational wave (GW) detector Virgo is approaching the end of the commissioning activities and the beginning of the long data taking, scheduled for 18 May 2007 [1]. The present detector data are characterized by a high-duty cycle and good stability, allowing us to test and setup the detection and veto algorithms and to tune the online and offline analyses pipelines. In these conditions it is possible to study the detector stability with respect to specific kinds of searches. In order to not interfere with the ongoing commissioning activity, since September 2006, the collection of science data takes place during the weekends. Such short runs are named weekly science runs (WSR). In this paper we present the status of the coalescing binaries (CB) search activities in Virgo. In addition, we show some results related to the WSR analysis with the CB pipelines and some aspects of the detector behavior.

2. Weekly science run

The periodic weekend data taking usually starts on Friday at 11 pm and ends on Monday at 7 am. In figure 1, the calendar of the six WSRs made in 2006 is reported. Two runs, taken during October 2006, have been canceled in advance.

The standard goal of these runs is to collect data in 'science mode' for 2.5 days, operating without any experiment or activity with the exception of calibration and hardware injections. During such runs we used the online analysis pipelines, processing the h-reconstruction and running both multi-band template analysis [2] and Merlino [3] codes. Produced results are stored for post-processing analysis. Part of the results are made available on the web, providing useful information about the events detection and the detector status. Acquiring data in controlled conditions permits us not only to exercise data analysis procedures but also gives important feedback to the commissioning team.

In figure 2, the sensitivity curve of the Virgo detector for some of the WSRs is plotted, together with the sensitivity of run C7 and the target sensitivity.

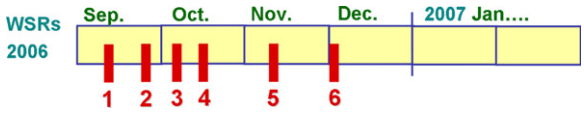

Figure 1. Weekly science run date: WSR1 (8–11 September 2006)—WSR2 (22–25 September 2006)—WSR3 (6–9 October 2006)—WSR4 (13–16 October 2006)—WSR5 (10–13 November 2006)—WSR6 (1–4 December 2006).

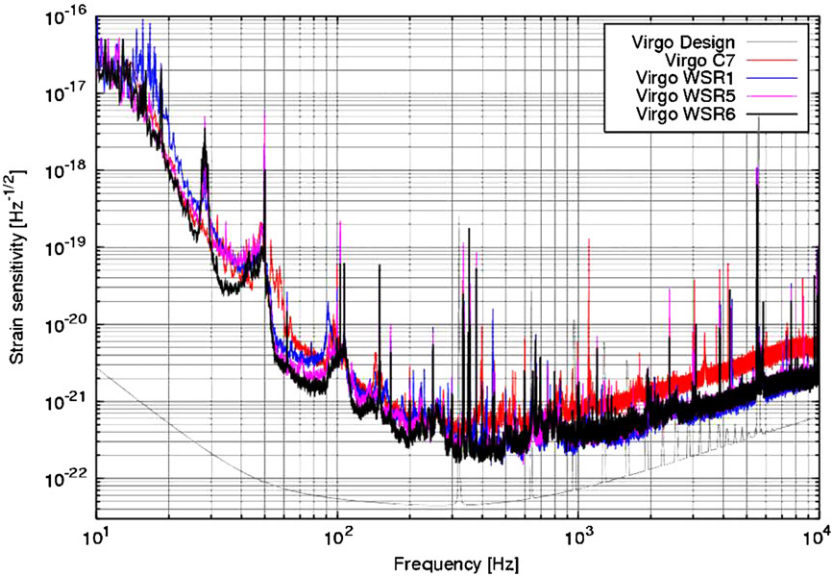

Figure 2. The Virgo sensitivities during C7, WSR1, WSR5, WSR6 are shown. The Virgo design sensitivity is also plotted.

3. Detector performance

It is convenient to describe detector performance in terms of duty cycle and horizon distance. The lock duty cycle is the percentage of time during which the interferometer is locked. In a similar way, we can define a science mode duty cycle as the time during which the interferometer is in the science mode.

The science mode duty cycle obtained during these runs was very promising. For WSR6 (see figure 3) the interferometer operated in the science mode 80.5% of the time. The best result was obtained in WSR1 with a duty cycle of 87.7%.

The horizon distance is one of the main indexes of the detector performance and corresponds to the distance of a coalescing binary system which would be detected with SNR=8. Usually, a binary system composed of two $1.4M\odot$ solar masses non-spinning NS is considered as a reference source to compute the horizon distance. Finally, two different measures of the horizon distance can be considered with the binary system optimally oriented or not[14].

In figure 3, we show the average horizon distance evolution during some of the weekly science runs. It is evident how we had significant horizon distance improvements between

[14] There, two definitions differ by the constant factor 2.3.

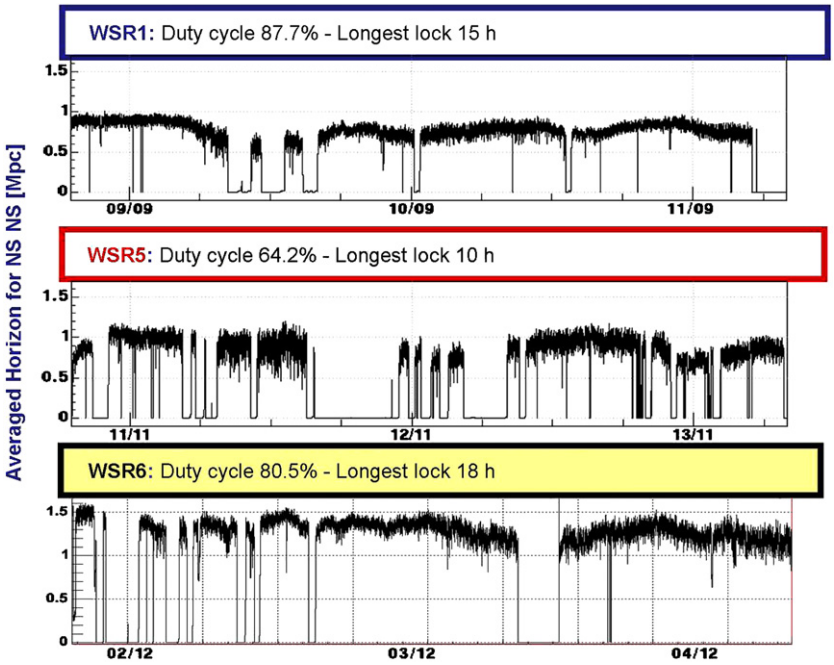

Figure 3. Average horizon distance during the most significative WSR for a $1.4/1.4 M_{\odot}$ NSNS binary with SNR = 8. The vertical scale is in Mpc. The science mode duty cycle is also reported in each panel.

WSR1 and WSR6, of the order of about 60%. In particular, in the last run we obtained an average horizon distance of 1.3 Mpc. The long locking periods are also evident with segments of 15–18 h. If the detector will keep the present stability and will significantly increase the horizon distance for the beginning of the long science run in May 2007, we will have good quality data to be used in the network of detectors analysis with LIGO detectors.

3.1. Horizon distance and environmental conditions

A dependency of the horizon distance from the seismic activity due to sea and wind has been noticed during the runs. Sea and wind activity are measured in microns using the Virgo suspension control system. An empirical relation between these two causes and the horizon distance was discovered, see figure 4. The relation is very simple: Horizon $= H_0(1 - a \times \mu\text{seism} - b \times \text{wind})$, where H_0, a, b are parameters and μseism and wind are the respective signals. In the top-right plot we show the sea activity, as a function of time, in the bottom-right plot we show the wind activity as a function of time, while in the left plot we show two overlapped curves: the black curve is the optimal horizon distance calculated starting as usual from the sensitivity, while the red curve is the horizon distance estimated combining the two seismic effects[15].

The horizon distance sometimes falls to zero. Such situations correspond to unlocks of the interferometer, that as we can see, are strongly correlated with seismic activity increase (see arrows).

[15] At the time of writing, this effect is no more observable, in particular after the improvements on the Virgo suspension controls.

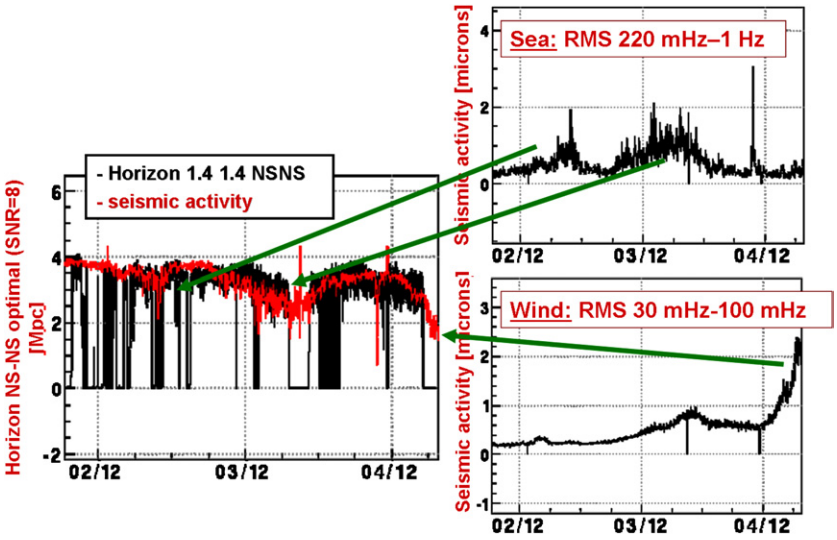

Figure 4. Upper right: time evolution of the RMS displacement (micron) in the range 0.22–1 Hz of the seismic activity due to the sea. Lower right: time evolution of the RMS displacement (micron) in the range 0.03–0.1 Hz of the seismic activity due to the wind. Both signals are obtained from the Virgo suspension control system. Left: optimal (i.e. for an optimally oriented binary system) horizon distance estimated using the detector sensitivity (in black) and estimated explicitly using the dependency on wind and sea.

4. CB triggers and detector behavior

As previously mentioned, the Virgo coalescing binaries group uses two main pipelines for the online analysis. These two pipelines share part of their code: in particular, the generation of the templates [4] and of the template grid [5]. Pipelines are configured to use a template bank covering the 0.9–3$M\odot$ masses range, using a minimal match of 98% and PN 2 approximation triggers are collected with a threshold of 6 in the signal-to-noise ratio.

Produced results are stored and used as a detector monitor. As a matter of fact, if the Virgo data stream diverges from Gaussianity in the frequency region of interest or if it is affected by glitches or other disturbances, these appear in the output stream as triggers. In the upper part of figure 5 the amplitude evolution of triggers, obtained during WSR2, is shown. In the lower part of figure 5 the output of a dark fringe at 1111 Hz for the same period is reported. Such signal accounts for the coupling between the frequency noise and the dark fringe signal. Comparing these two plots, a close correlation between the trigger's signal-to-noise ratio and the frequency noise is evident. We note that the amplitude of the recorded trigger was characterized by good stability for a large part of the run, due to the presence of few peaks with high amplitude. The situation was different in the last part of the data taking (highlighted with a dashed box in figure 5) where the detector noise increased, leading to higher signals.

In figure 6 we show the spectra of the triggers sequence. This plot provides useful information about the various contributions coming from different frequencies and about signal stationarity. As an example we can observe the 0.2 Hz peak, which is correlated with the micro-seismic activity.

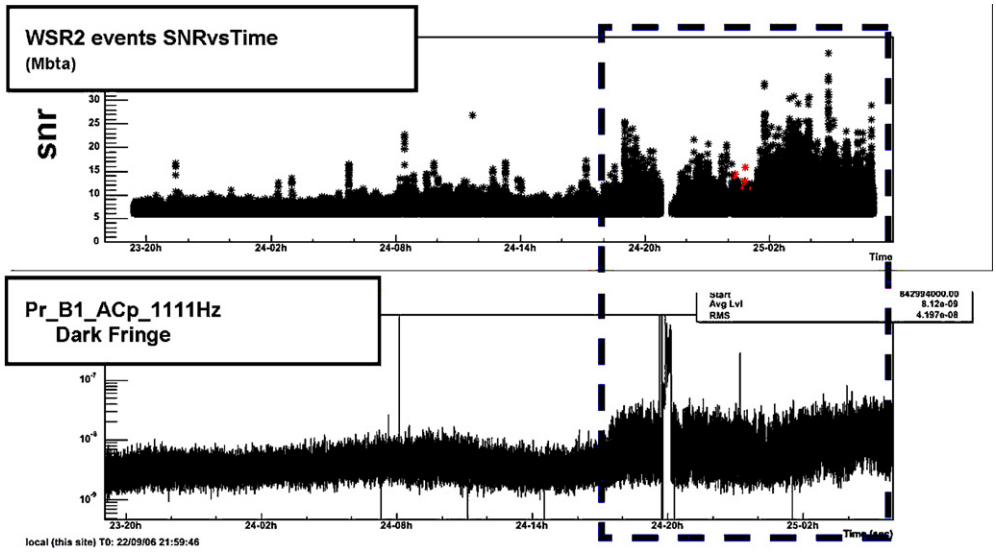

Figure 5. Upper plot: the evolution of the triggers amplitude (SNR) detected using MBTA during WSR2. Lower plot: output of the Virgo main stream, read with the B1_Cap acquisition channel at 1111 Hz.

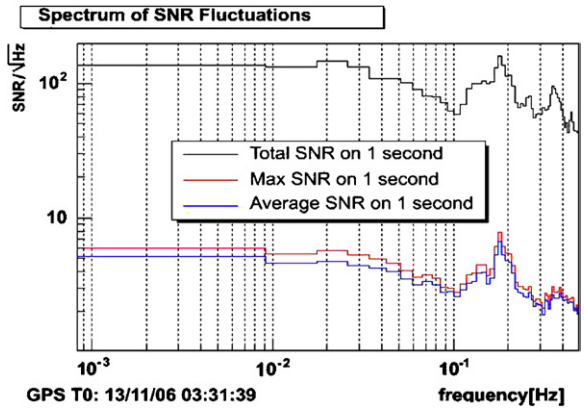

Figure 6. The spectrum of the trigger time series of the WSR2 is reported. It is visible that the 0.2 Hz peak is correlated with the microseismic activity effect.

5. Hardware injections

The injection of supernova and coalescing binary signals via hardware into the Virgo interferometer is one of the main WSR duties. This activity is performed in the first and the last nights of the run, with the aim of simulating GW effects on the detector and testing the detection pipelines.

Injections are performed acting on the input mirror of the north Fabry–Perot cavity. A properly shaped force is applied to the test masses, taking into account the electromechanical response of the mirror suspensions. The injected signals are generated, using a PN 2 approximation, considering a $1.39M\odot$–$1.47M\odot$ non-spinning NS binary system, with a

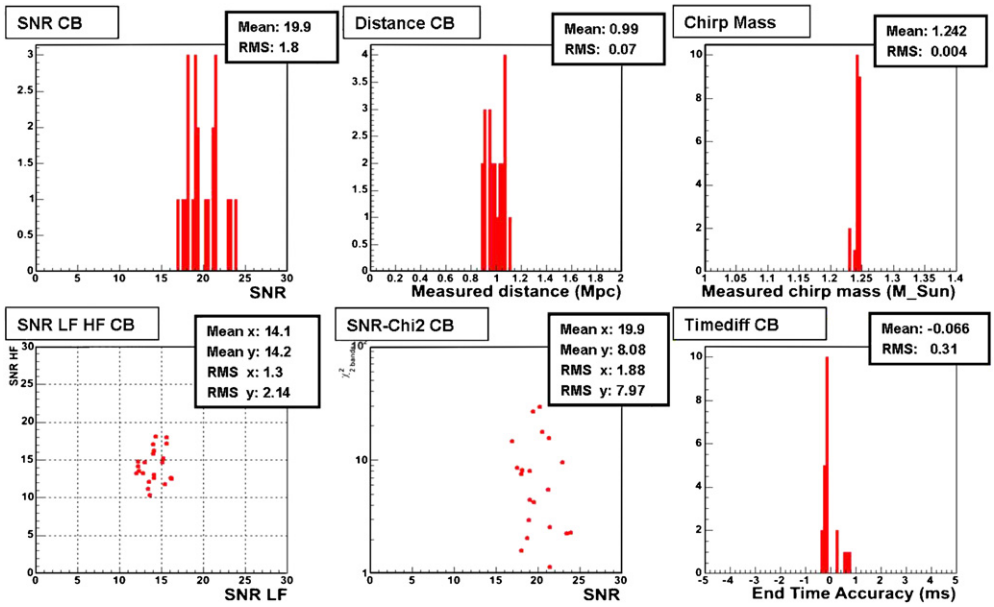

Figure 7. We show an example of parameter reconstruction, using the hardware injection made in WSR6 and the MBTA analysis code.

lower frequency cut-off of 50 Hz, optimally oriented with respect to the detector, and located at a nominal distance of 1.08 Mpc[16]. The nominal distance has been computed using the sensitivity measured at the time of the injections.

The data containing injections are analyzed by the CB pipelines to check detection efficiency and accuracy in parameter reconstruction. In figure 7 an example of parameter reconstruction with the WSR6 data is shown. For brevity we consider only MBTA events, because results obtained with the Merlino pipeline are similar.

As can be seen the chirp mass and time accuracy are very well reconstructed. Detailed results on time accuracy have been reported in [8] where we show how the timing of inspiral signals can be improved using a reference time at a frequency different from the usual time definition.

We found a discrepancy between the reconstructed distances and the real ones. The reconstructed distance had a mean value of 0.99 Mpc, while the expected value was 1.08 Mpc. We noted that both MBTA and Merlino pipelines recorded the same result. The reason was found to be associated with a calibration error due to failure in the actuation electronics.

MBTA uses two template families, one for the higher frequency band and the other for the lower frequency band. In the bottom-left of figure 7 the SNR for each band for all the detected events are shown, confirming the equal distribution of the detected SNR between the two bands. Hence energy is approximatively equally distributed across the bands for each event, with a value of the order of 15 per band.

6. Veto

It is important to implement efficient methods in order to reduce this percentage and to select out real triggers produced by coalescing binaries events. For this aim both pipelines use an

[16] The event distance is kept fixed during the injections while the event SNR changes with the detector sensitivity.

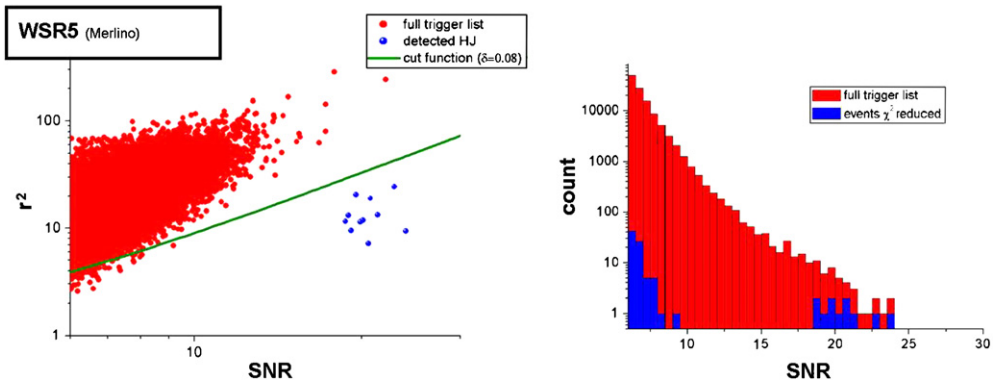

Figure 8. Left: the SNR-χ^2 scatter plot is reported, using the WSR5 results. Also the detected hardware injections with SNR around 20, and the cut function used to discriminate the events, are shown. Right: presents the histogram of the triggers SNR: in red the full trigger list is reported, while in blue the residual list of events below the function $(1 + 0.08\rho^2)$ is reported.

online χ^2 time/frequency veto [6]. MBTA implements a χ^2 with two bands, estimated without specific computation, using the information already available from the two bands. Merlino applies a specific plug-in for the χ^2, configured with 15 bands, giving a higher veto efficiency. A higher computational overhead is the price paid for this gain.

In the left plot of figure 8, we show as an example the SNR versus χ^2 obtained during WSR5 with the Merlino pipeline. In the plot, the group of signals with a signal-to-noise ratio around 20 is associated with CB injections. Due to the high energy of the injections, they appear to be quite separable from all the other signals associated with noisy events.

In order to use this result as a veto, we identify a rejection area in such a plot, cutting the space SNRχ^2 with a suitable function. As reported in [7], in the presence of Gaussian noise a quadratic function of the SNR $(1 + \delta\rho^2)$ is used, where ρ is the SNR of the event and δ is a parameter, whose value depends on the required false alarm rate. Applying this veto to the trigger populations, it is possible to drastically reduce the number of false events. In the right plot we show in red the SNR histogram of the original events list and in blue the list of triggers surviving the χ^2 veto procedure. In this case we used $\delta = 0.08$. The group of injected CB signals is clearly visible, well separated from the triggers associated with noise. In Virgo we perform systematic tests on such type of veto, using not only hardware injections but also software injections, covering a wider signals family. With lower SNR (less than 8) the veto efficiency is significantly reduced and for that it is important to estimate the receiver operative characteristics with software simulations.

Other veto procedures are possible and have been identified, in particular for what concerns the data quality definition. We implement an *a priori* veto, such as a monitor for saturation in coil current in the NE and WE towers, a monitor for picomotors and a monitor for second stage of frequency stabilization saturation. We are also working on the definition and testing of *a posteriori* veto. A promising one is the B2 veto that monitors the power variation in the cavities with the B2 channel signal. In figure 9 we show an example of such a veto application, using the WSR2 results. In the left panel the SNR histogram of the full trigger list is reported. In the right panel the SNR histogram of the triggers surviving the B2 veto is reported. In red we identify the CB injected signals. In this case we have a reduction of false alarm of about $\approx$10%, removing principally high SNR triggers.

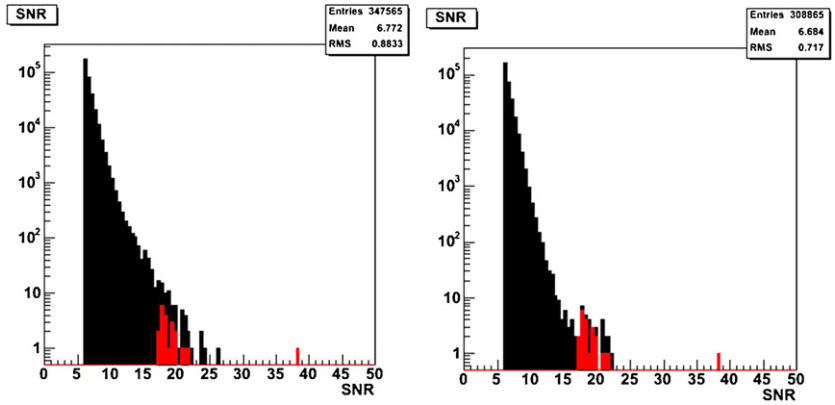

Figure 9. We show an example of the B2 veto application on the WSR2 data. Left: the SNR distribution of the full trigger list is reported. Right: the SNR distribution of the triggers, surviving the B2 veto, is reported. We highlight the events associated with the detected hardware injections in red.

7. Conclusions

In 2006 the Virgo collaboration decided to periodically start a number of short science runs (called weekly science runs) in order to collect useful information for data analysis and commissioning activities. Detector data were characterized by a high-duty cycle and a general good stability, allowing us to test and setup the detection and veto algorithms for the online and offline analyses. In this paper we reported a number of results obtained by the Virgo coalescing binary group. In particular, we presented some results obtained with MBTA and Merlino detection pipelines, concerning the use of veto techniques and the accuracy in parameter reconstruction using hardware injections.

References

[1] Acernese F *et al* (The Virgo collaboration) Status of Virgo detector *Class. Quantum Grav.* **24** S381–8
[2] Marion F *et al* (The Virgo collaboration) 2004 Gravitational waves and experimental gravity *Proc. Rencontres de Moriond, Les Arcs, France, March 2003*
[3] Amico P *et al Comput. Phys. Commun.* **153** 179–89
[4] Bosi L *et al* 2004 *The Inspiral Library User Manual* A
[5] Beauville F *et al* 2003 *Class. Quantum Grav.* **20** S789A
[6] Allen B *Phys. Rev.* D **71** 062001
[7] Allen B *et al* 2005 FINDCHIRP: an algorithm for detection of gravitational waves from inspiraling compact binaries *Preprint* gr-qc/0509116
[8] Acernese F *et al* (The Virgo collaboration) Improving the timing precision for inspiral signals found by interferometric gravitational wave detectors *Class. Quantum Grav.* **24** S617–26